Coarse-Grained Force Field for Lipid Domain Formation Simulations

Sangjae Seo, and Wataru Shinoda
Department of Materials Chemistry, Nagoya University,
Furo-cho, Chikusa-ku, Nagoya, 464-8603

1. Introduction

During the last decades, the structure of cellular membrane has gained lots of attentions due to its biological importance [1]. Especially, the functions and existence of lipid raft in the plasma membrane have been intensively studied by experiments, theories, and computer simulations. The lipid raft model suggests that the biological membrane is not homogeneous, rather separated into liquid ordered (L_o) and disordered (L_d) domains mostly due to the different affinity of cholesterol (Chol) between saturated and unsaturated lipids. Experimentally, the fluorescent microscopes have revealed the existence of lipid raft in the model vesicles, which have simple compositions [2, 3]. However, despite of the enormous effort to reveal the structure of lipid raft *in vivo*, our knowledge is still limited due to its size and dynamic nature. In this regard, molecular dynamics (MD) simulation has been extensively exploited to study the membrane structure. MD simulation gives insightful information in atomic resolutions by numerically solving the Newton's equation of motion for atoms. The forces acting on each particle are calculated based upon the force field (FF), which contains a set of parameters of empirical potential function. Since the accuracy of the MD simulation results rely on the quality of FF, it is of great importance to develop accurate FF. Recent all-atom (AA) FFs, which are generally fitted to the quantum mechanical data, provides accurate structural properties of lipids [4, 5]. However, because AA FF requires expensive computational costs, it is not eligible to investigate the phase separation of lipid membrane. Coarse-grained (CG) FFs exploit less detailed description of atoms. Several heavy atoms are mapped into one single bead, so that it can easily reduce the number of interactions. In this report, we will shortly introduce the available CG FFs, and our recent development of CG FF for the purpose of phase separation simulation.

1.1. Coarse-grained force fields

MARTINI is one of the most successful CG FF for the simulation of biomolecules [6, 7]. Generally, four heavy atoms are represented by a single CG site. MARTINI FF has fixed number of CG sites, and the interactions between CG sites were determined by the reproduction of partitioning free energies. Since the available CG bead types are predefined, such as polar, nonpolar, apolar, and charged, user can readily create a CG model of new molecule without any further parameterization process. However, due to the fixed number of CG bead types and constrained σ value (*i.e.*, σ=0.47 nm) of Lennard-Jones (LJ) interaction, the accuracy is not always guaranteed.

Iterative Boltzmann inversion (IBI) method derives the CG interactions from the structural data retrieved from the fine grained model [8]. The radial distribution function (RDF) obtained from the AA MD simulation is targeted. RDF is converted into the interaction potential by Boltzmann inversion, and iteratively updating trial potential, finally the tabulated potential for interaction is determined. Although IBI is a systematic way to determine the parameters, because IBI only accounts for the structural aspect, the thermodynamic properties are poorly

described.

Shinoda-DeVane-Klein (SDK) model was designed to accurately predict the interfacial properties [9, 10]. The parameters were optimized against the thermodynamic properties, and SDK model can accurately reproduce the membrane properties. However, the previous cholesterol model developed in the SDK was not successful to show the phase separation of lipid mixtures in the same condition to the experiment [11]. In this study, we developed a new CG FF, coined SPICA FF, which can accurately predict the phase behavior, in the spirit of SDK model [12].

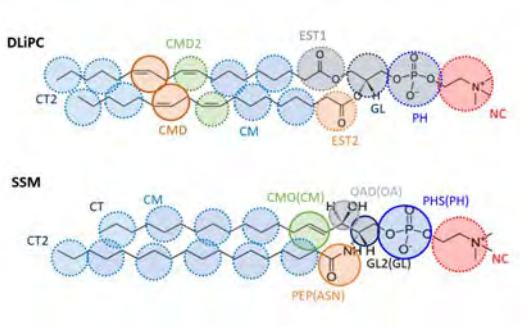

Fig. 1: CG Mapping of DLiPC and SM lipid. Solid circle indicates the new bead developed in this study and dashed circles are taken from SDK model. The name of bead type in the parenthesis is the similar bead taken from the SDK model.

2. Methods

2.1. Modeling and parameterization

SPICA FF was developed as an extension of SDK model. We added new lipid types; sphingomyelin (SM) and polyunsaturated lipids, and optimized the Chol parameters to accurately reproduce the structural properties. CG mapping scheme and resolution followed that of the SDK model. Three to four heavy atoms of lipid molecules were mapped into CG beads. Figure 1 depicts the CG mapping of SM and DLiPC. Functional groups, such as hydroxyl group, and amino group, were mapped into one CG bead.

SPICA FF exploits the same functional form of the potential functions used in the SDK model. The bonded interactions are defined as,

$$U_{\text{bonded}} = \sum_{\text{bond}} k_b (r_{ij} - r_0)^2 + \sum_{\text{angle}} k_\theta (\theta_{ijk} - \theta_0)^2 + \sum_{\text{dihed}} k_\phi \left[1 + \cos\left(n\phi_{ijkl} - d\right)\right] \quad (1)$$

For the angle parameter, in order to avoid angle collapse, additional Lennard-Jones (LJ) type interaction is sometimes added.

$$U_{1-3}^{\text{correct}} = \sum_{1-3} \left[U_{nb}\left(r_{ij}\right) - U_{nb}\left(r_{\min}\right)\right] \quad \text{for} \quad r_{ij} < r_{\min} \quad (2)$$

We determined the parameters of bonded interaction by fitting to the distribution obtained from the AA MD simulation. The non-bonded interaction is defined as;

$$U_{nb}(r_{ij}) = \begin{cases} \frac{3\sqrt{3}}{2}\varepsilon_{ij}\left[\left(\frac{\sigma_{ij}}{r_{ij}}\right)^{12} - \left(\frac{\sigma_{ij}}{r_{ij}}\right)^{4}\right] & \text{for the pairs involving water} \\ \frac{27}{4}\varepsilon_{ij}\left[\left(\frac{\sigma_{ij}}{r_{ij}}\right)^{9} - \left(\frac{\sigma_{ij}}{r_{ij}}\right)^{6}\right] & \text{for any other pairs} \end{cases} \quad (3)$$

Basically, the non-bonded interactions were determined to satisfy surface tension and density of analogue molecules. For the cross interactions (between different bead types), the σ values were easily determined by the Lorentz-Berthelot rule, $\sigma_{ij} = \frac{\sigma_{ii} + \sigma_{jj}}{2}$. However, fitting to such thermodynamic properties could not decide most of ε values of cross interactions because it does not follow the conventional combination rule. Thus, for lipid molecules, the remaining

cross interactions were optimized by targeting membrane properties, such as membrane area, thickness, area compressibility modulus. Moreover, for the optimization of Chol model, in order to make Chols correctly partition in the mixture systems, 2D RDF was also considered. Namely, we calculated 2D RDF of Chol-lipid in lipid membranes for a series of different concentration of Chol from AA MD simulations, which were used as reference data for the optimization of CG parameters.

Since there was no systematic way to determine the parameters that simultaneously satisfy the membrane properties, we explored the parameters by random searching. To reflect the chemical interaction, we multiplied the scaling value, *k*, to the conventional combination rule, $\varepsilon_{ij} = k\sqrt{\varepsilon_{ii}\varepsilon_{jj}}$, and created a huge number of parameter sets, which have various scaling values for each interaction. Then, we chose the best parameter set, which most accurately reproduce all the target membrane properties.

2.2. Molecular dynamics simulation

We conducted both AA and CG MD simulations. AA MD simulations were conducted using NAMD package with the CHARMM36 FF [4] to produce the reference data. The AA MD simulations were run for 1 μs at 323K and 1atm controlled by Langevin dynamics and Nosé-Hoover Langevin piston, respectively. CG MD simulations were conducted using LAMMPS for 500 ns to calculate the membrane properties. Nosé-Hoover thermostat and Parrinello-Rahman barostat were used to maintain the temperature and pressure at 323K and 1atm, respectively. For ternary mixture systems, the temperature was set at 298K, which is the same condition as the experiments.

The initial structures were prepared by the CHARMM-GUI [13]. In case of ternary mixtures, the small patches created by CHARMM-GUI were duplicated to generate large membrane.

2.3. Analyses

We measured the various membrane properties to assess the SPICA FF. Area per lipid was measured by dividing the simulation box size by the number of lipids. The thickness of membrane was defined as the average phosphate-phosphate distance. The area compressibility was calculated by

$$K_A = \frac{k_B T \langle A \rangle}{N \sigma^2_{\langle A \rangle}} \tag{4}$$

where $< A >$ and $\sigma^2_{<A>}$ are the average surface area and the dispersion, respectively. The segmental order parameter was calculated by

$$S_{ZZ} = \frac{\left\langle 3\cos^2\theta - 1 \right\rangle}{2} \tag{5}$$

where θ is the angle between membrane normal and the vector connecting consecutive hydrophobic tail beads.

For the phase separation simulation, we quantified the degrees of phase separation by the contact ratio, which is defined as

$$\Phi_C = \frac{N_{chol-sat}}{N_{chol-sat} + N_{chol-unsat}} \tag{6}$$

where $N_{x\text{-}y}$ is the number of contacts between *x*-lipid type and *y*-lipid type. We counted the number of contacts in the shared edged from the Voronoi tessellation.

3. Results and Discussion

3.1. Membrane properties

We evaluated the quality of SPICA FF by comparing the membrane properties to the AA simulations and experimental results. Table. 1 lists calculated membrane properties of area, thickness, and area compressibility. The membrane properties of unitary membrane show good agreement with AA MD result.

Lipid	SA/lipid [Å^2]		Thickness [Å]		K_A [mN/m]	
	AA	CG	AA	CG	AA	CG
SSM	54.4	57.2	43.1	41.4	440	460
PSM	55.4	56.8	40.7	39.6	350	460
DLiPC	70.2	71.3	36.9	36.9	263	357

Table 1: Calculated membrane properties of unitary membranes. Errors of SA/lipid and thickness are less than ±1%, and K_A is less than 10%.

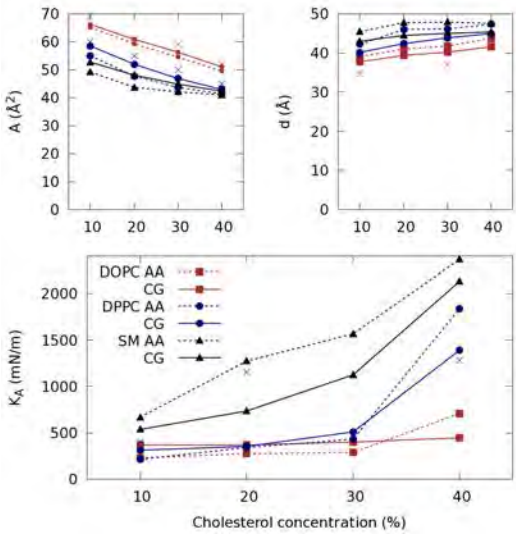

Fig. 2: Membrane properties containing Chol.

Figure 2 displays the membrane properties of binary mixtures containing various Chols contents. Similar to the unitary systems, the results of CG MD simulations of binary mixtures are well agreed with the AA MD simulation results. The condensing effect and ordering effects, which are evidenced by the smaller area and larger thickness in the higher Chol concentration, are well reproduced by the SPICA force field.

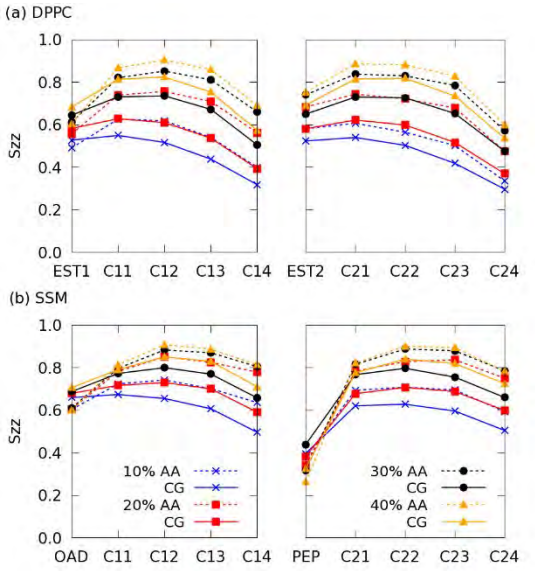

Fig. 3: Order parameters of membranes containing Chol.

The order parameter of CHARMM FF was extensively evaluated by comparing to the experimental values, and it has been shown that CHARMM can accurately reproduce the S_{CD} value [4]. Since we cannot directly evaluate the S_{CD} value from CG MD, we calculated the CGed segmental order parameter, S_{ZZ}, (Eq.(5)) instead, and compared between AA and CG MD simulations. As shown in Fig. 3, although *Szz* values of CG MD simulation are slightly lower than that of AA MD simulation, the overall agreement is still satisfactory and the *Szz* variation as a function of chol concentration is also reproduced. The ordering effect of Chol is

clearly shown by higher order parameters in the higher Chol concentrations.

We also paid extra attentions to the Chol distribution. We plot the 2D RDF and compared with AA MD simulation result (Fig. 4). In case of DOPC membrane, the RDF plots of Chol almost coincide with AA simulation result. The locations and height of each peak are well reproduced by SPICA FF.

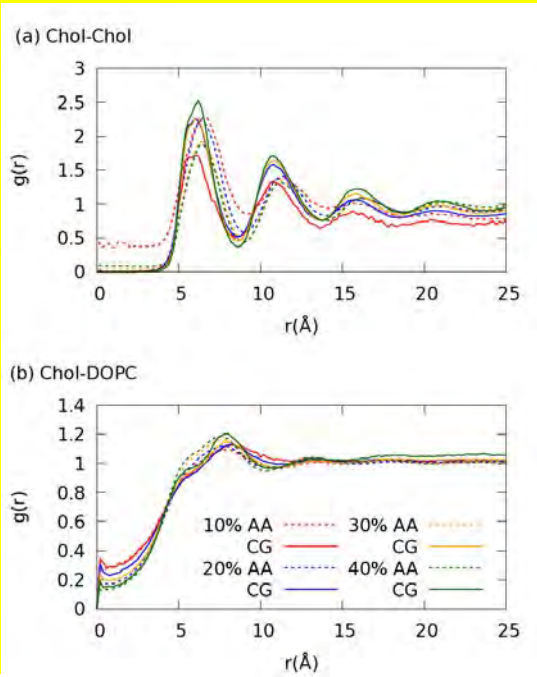

Fig. 4: 2D RDFs of each pair in DOPC membrane containing Chol. (a) Pair of Chol-Chol, and (b) Chol-DOPC

In addition to the 2D RDF, we also checked the Chol distribution with respect to the Chol faces. Chol has two faces; α-face is a flat surface, and β-face is a rough surface containing protruded methyl group. Due to the asymmetric structure of Chol, it has been known that the Chol distribution shows three-fold symmetry. Figure 5 shows the in-plane Chol distribution with respect to the reference orientation of Chol. First, the highlights correspond to the peaks in the 2D RDF curves. In case of AA MD simulation, one can observe the three hot spots pointed by the red arrows, which indicates the three-fold symmetry. Although the Chol model of SPICA failed to reproduce 3-faces, the overall distribution on α-face and β-face is still well reproduced.

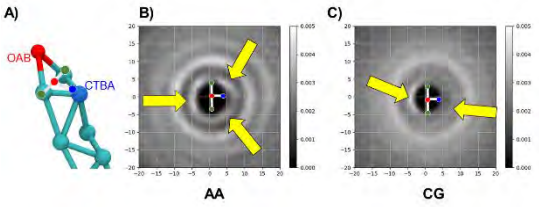

Fig. 5: In-plane probability distribution of Chols. (a) Schematic description of the orientation. (b-c) Arrows indicate the three-, and two-fold symmetry.

3.2. Phase separation simulation

One of the main goals of the development of the SPICA FF was to accurately reproduce the phase behavior in the ternary mixture. As mentioned above, the stronger interaction between Chols and saturated lipids leads to the phase separation of L_o and L_d domains. First, we evaluated the chemical potential of Chol in different lipid membranes. One Chol molecule in the lipid bilayer was pulled from the equilibrium position to the water region, and the required free energy was calculated by the adaptive biasing force method [14]. As Fig 6 depicts, the free energy difference between in the lipid bilayer and water region. Smaller free energy difference at higher Chol concentration indicates that Chols prefer the higher concentrations regardless of the lipid type. In addition, Chol shows preferred interaction with saturated lipid, such as SSM and DPPC. The chemical potential difference between DOPC and saturated lipid suggests that Chol prefers to stay in the saturated lipid domain

and the trend is accelerated as increasing Chol concentration, which leads to the phase separation.

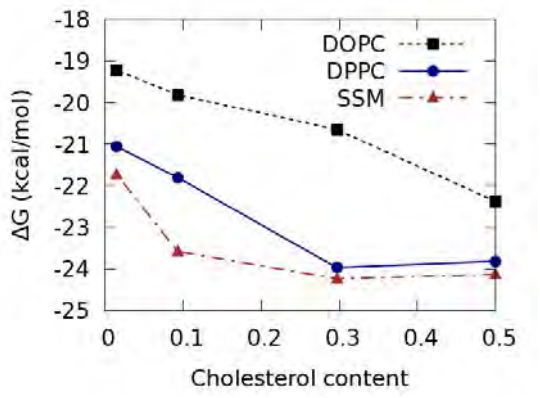

Fig. 6: Chemical potential of Chols in different lipid membrane.

We simulated the ternary mixture of DOPC, DPPC and Chol (DPPC-DOPC-CHOL) in 1:1:1 ratio. This composition extensively investigated by the fluorescent experiments has been shown macroscopic phase separations. However, the MARTINI FF has failed to obtain the phase separation of this mixture. We have carried out a CG-MD simulation of the DPPC-DOPC-CHOL mixture for 4 μs and succeeded in showing a phase separation. As shown in Fig. 7, the membrane was phase separated into L_o region enriched with DPPC and Chol, and L_d region mostly consisted with DOPC. The contact ratio increased up to 0.8, which clearly indicated the enrichment of Chols in the DPPC region.

We also tested the polyunsaturated lipid for the phase separation. The CG MD simulation of the mixture of DPPC, DLiPC, and Chol (DPPC-DLiPC-Chol) was conducted for 4 μs. Similar to the membrane of DPPC-DOPC-CHOL, DPPC-DLiPC-Chol membrane was also phase separated. Interestingly, the membrane showed anti-registered (phase asymmetric) domain separation. We speculated that the large hydrophobic mismatch leads to the anti-registration. The average thickness of L_o

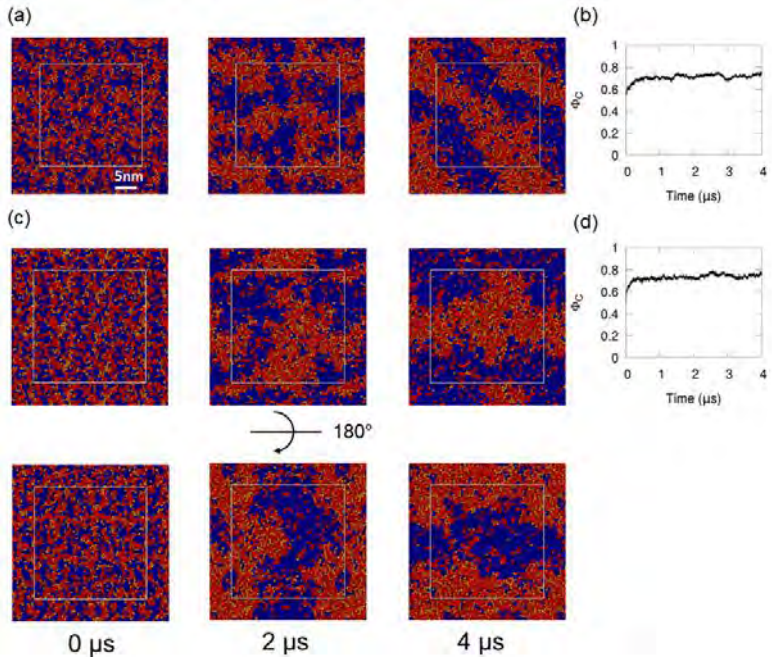

Fig. 7: Snapshots of phase separation in the course of simulation. (a-b) DPPC-DOPC-Chol, (c-d) DPPC-DLiPC-Chol.

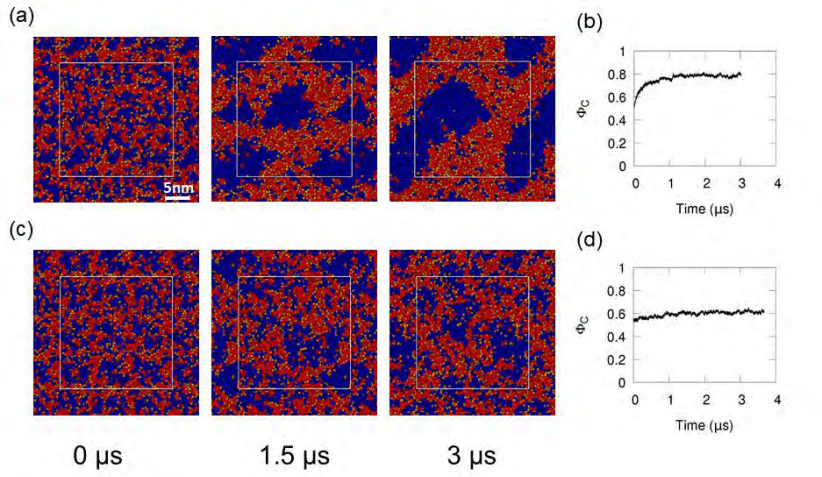

Fig. 8: Snapshots of phase separation in the course of simulation. (a-b) SSM-DOPC-Chol, (c-d) SSM-POPC-Chol.

domains enriched with DPPC and Chol increases up to 44 Å, whereas, L_d domains, mostly consisting DLiPC is only about 37 Å. Thus, the large hydrophobic mismatch between L_o and L_d domain may give rise to the anti-registration to minimize the hydrophobic mismatch energy.

Since SM lipids are generally accepted as the main lipid type induces the phase separation in the plasma membrane, we also run the CG MD simulation of the mixture of SSM, DOPC, and Chol (SSM-DOPC-CHOL). Experimentally, it already has shown that the ternary mixture of SSM-DOPC-CHOL shows the macroscopic phase separation [2]. Figure 8 displays the phase behavior in the course of the simulation. Similar to experimental results, the mixture showed phase separations after 4 μs. The contact ratio increased up to 0.8. Also, it has been experimentally shown that the replacement of DOPC to POPC leads to the conversion from macroscopic phase separation to microscopic phase separation [2]. We could observe the same phenomenon. As shown in Fig 8, in case of SSM-POPC-CHOL, the domain size after the phase separation is much reduced and the membrane shows ambiguous domain boundaries. It was also confirmed in the contact ratio plot. Although the contact ratio slight rises at the initial step of phase separation, the value was saturated at ~0.6. This clearly indicates the disruption of domains because of the replacement of unsaturated lipid.

4. Conclusion

Accurate prediction of phase separation using CG MD simulation is important to understand underlying mechanism of lipid raft formation. In this research, we developed a new coarse-grained force field, called SPICA, which can accurately reproduce the membrane properties and phase behavior. The parameters were fitted against the membrane area, thickness, and area compressibility modulus. More importantly, the Chol model was highly optimized against RDF, so that the Chol partitioning in the mixture was accurately calculated. Then, we ran a series of CG MD simulations of the ternary mixtures consisting saturated lipid, unsaturated lipid, and Chol. The phase behavior observed from the CG

MD simulation was consistent with experimental result. Interestingly, we found that the significant hydrophobic mismatch gives rise to the anti-registration. We expect that the SPICA FF developed in this research will enable us to understand the lipid raft and membrane structure. The FF parameters are provided on the official website, http://spica-ff.org/. An extension of SPICA FF for proteins are now underway. We are going to publish the FF in near future.

References

[1] K. Simons and E. Ikonen, Nature, **387** (1997) 569-572.

[2] S.L. Veatch and S.L. Keller, Biophys. J., **85** (2003) 3074-3083.

[3] T. Baumgart, S.T. Hess, and W.W. Webb, Nature, **425** (2003) 821-824.

[4] J.B. Klauda, et al., J. Phys. Chem. B, **114** (2010) 7830-7843.

[5] J.P.M. Jämbeck and A.P. Lyubartsev, J. Chem. Theory Comput., **9** (2012) 774-784.

[6] S.J. Marrink, et al., J. Phys. Chem. B, **111** (2007) 7812-7824.

[7] M.N. Melo, H.I. Ingólfsson, and S.J. Marrink, J. Chem. Phys., **143** (2015).

[8] D. Reith, M. Pütz, and F. Müller-Plathe, J. Comput. Chem., **24** (2003) 1624-1636.

[9] W. Shinoda, R. DeVane, and M.L. Klein, Mol. Simul., **33** (2007) 27-36.

[10] W. Shinoda, R. DeVane, and M.L. Klein, J. Phys. Chem. B, **114** (2010) 6836-6849.

[11] C.M. MacDermaid, et al., J. Chem. Phys., **143** (2015).

[12] S. Seo and W. Shinoda, J. Chem. Theory Comput., **15** (2018) 762-774.

[13] J. Lee, et al., J. Chem. Theory Comput., **12** (2015) 405-413.

[14] E. Darve, D. Rodríguez-Gómez, and A. Pohorille, J. Chem. Phys., **128** (2008).